

SatelliteFormula: Multi-Modal Symbolic Regression from Remote Sensing Imagery for Physics Discovery

Zhenyu Yu
Universiti Malaya
yuzhenyuyxl@foxmail.com

Mohd. Yamani Idna Idris
Universiti Malaya

Pei Wang
Kunming University of
Science and Technology

Yuelong Xia
Yunnan Normal University

Fei Ma
Guangming Laboratory

Rizwan Qureshi
University of Central Florida

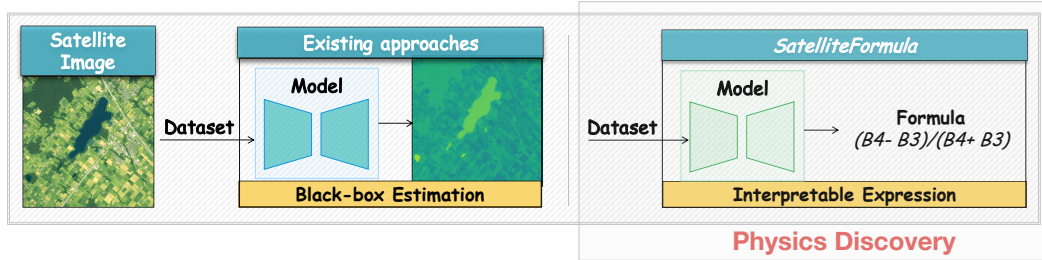


Figure 1: Motivation. Traditional methods rely on black-box models for estimation, lacking interpretability and physical insights. In contrast, *SatelliteFormula* directly infers symbolic expressions from satellite imagery, enabling physics discovery.

Abstract

We propose *SatelliteFormula*, a novel symbolic regression framework that derives physically interpretable expressions directly from multi-spectral remote sensing imagery. Unlike traditional empirical indices or black-box learning models, *SatelliteFormula* combines a Vision Transformer-based encoder for spatial-spectral feature extraction with physics-guided constraints to ensure consistency and interpretability. Existing symbolic regression methods struggle with the high-dimensional complexity of multi-spectral data; our method addresses this by integrating transformer representations into a symbolic optimizer that balances accuracy and physical plausibility. Extensive experiments on benchmark datasets and remote sensing tasks demonstrate superior performance, stability, and generalization compared to state-of-the-art baselines. *SatelliteFormula* enables interpretable modeling of complex environmental variables, bridging the gap between data-driven learning and physical understanding.

1 Introduction

Remote sensing imagery provides rich multi-spectral data critical for assessing vegetation health, soil moisture, and surface temperature [7, 59, 37]. While traditional indices (e.g., NDVI, SAVI) rely on expert-designed formulas [36, 53, 58], and deep learning models (e.g., Transformers, UNet, GNNs) offer strong predictive power [15, 54], both approaches fall short in deriving explicit, physically interpretable expressions. Symbolic Regression (SR) has emerged as a compelling alternative, capable of uncovering latent physical laws [24, 57]. However, applying SR to remote sensing is hindered by

the high-dimensional and spatial-spectral complexity of satellite data [21, 46]. The central **problem** remains: how can we directly infer physically grounded expressions from raw imagery? Solving this would significantly enhance environmental monitoring and scientific interpretability in geospatial analysis [11].

Symbolic regression (SR) has progressed from early Genetic Programming (GP) approaches—capable of discovering closed-form expressions but limited by computational inefficiency in high-dimensional settings [48, 49, 51]—to physics-informed frameworks like AI Feynman and PINNs, which integrate domain constraints for improved interpretability but remain restricted to tabular data [38, 60, 52, 55]. Recent Transformer-based models (e.g., SymbolicGPT, NeSymReS, TPSR) have enabled scalable and efficient expression discovery through sequence modeling of symbolic forms [41, 33, 45]. Building on these advances, Multi-Modal Symbolic Regression (MMSR) has emerged to address the broader challenge of extracting interpretable expressions from multi-modal inputs [27, 56].

Challenges. Despite MMSR’s ability to handle multi-modal data, its data encoder remains optimized for numerical tabular data, making it challenging to effectively capture the complex spatial and spectral features present in remote sensing imagery [32, 31]. Multi-spectral data often exhibit high spatial dependencies and spectral variance, which traditional encoding mechanisms struggle to learn [17, 54]. This limitation not only affects the accuracy of physical modeling but also hinders the applicability to more advanced geospatial tasks [13].

Our Approach. To overcome the limitations of prior SR methods on remote sensing data, we introduce *SatelliteFormula*, a symbolic regression framework tailored for multi-spectral imagery. Unlike existing approaches reliant on tabular data or handcrafted features, *SatelliteFormula* directly operates on image inputs via a dedicated image encoder that captures fine-grained spatial and spectral patterns critical for physics-aware modeling.

Key Contributions.

- We propose *SatelliteFormula*, the first symbolic regression framework to derive physically interpretable expressions directly from multi-spectral remote sensing imagery.
- We design a multi-spectral image encoder that preserves both spatial structure and spectral variance for symbolic inference.
- We introduce physics-based constraints via a physical loss, enabling selection of expressions consistent with known physical principles.

2 Related Work

2.1 Traditional Symbolic Regression Methods

Symbolic regression (SR), based in Genetic Programming (GP), has long been used for interpretable scientific discovery [20]. GP evolves mathematical expressions to fit data but suffers from high computational cost, limited scalability, and a tendency toward overly complex or suboptimal expressions [29]. While its interpretability is appealing, these limitations hinder its effectiveness on modern, high-dimensional datasets. Recent efforts have improved scalability by integrating meta-learning and neural-guided search [50]. To overcome GP’s limitations, physics-guided symbolic regression methods such as AI Feynman [39] and SINDy [5] integrate domain knowledge to constrain the search space and enhance interpretability. AI Feynman applies dimensional analysis, while SINDy identifies sparse representations of dynamical systems. Although effective for tabular data, these methods lack support for complex multi-modal inputs like remote sensing imagery. Hybrid approaches combining physics-informed neural networks (PINNs) with symbolic regression aim to address this gap, but still struggle with spatial and spectral dependencies inherent in high-dimensional image data [44].

2.2 Transformer-based Symbolic Regression

Transformer architectures have redefined symbolic regression by framing expression generation as a sequence modeling task, offering greater scalability and efficiency than GP-based approaches [42]. For example, SymbolicGPT [18] treats symbolic expression generation as a language modeling problem, generating token-by-token expressions to capture mathematical structure. Although, it

outperforms traditional SR methods in accuracy and complexity [40], it incurs high training costs for large input spaces. Recent variants incorporate sparse attention to reduce overhead [34]. TPSR [22] combines Transformer decoding with Monte Carlo Tree Search (MCTS) to efficiently explore expression trees and prune redundancies. However, its architecture remains limited in handling heterogeneous data modalities [47].

NeSymReS [3] achieves strong generalization through pretraining on large symbolic corpora. While effective on tabular benchmarks, its original design is not optimized for spatial or multi-modal data. Recent extensions explore multi-task learning to broaden its applicability [27]. Despite these advances, Transformer-based symbolic regression methods have not fully explored applications to multi-modal data such as remote sensing imagery, underscoring the need for a novel framework capable of handling spatial and spectral dependencies [17].

2.3 Symbolic Regression for Remote Sensing

Remote sensing analysis has traditionally relied on handcrafted empirical indices such as NDVI and SAVI [16], which are tailored to specific spectral bands and exhibit limited generalizability. Black-box models like Random Forest and XGBoost [6] excel in predictive tasks but lack interpretability and the ability to uncover physical laws. Similarly, convolutional neural networks [61] and probabilistic programming approaches [10] have been explored for remote sensing but struggle to balance interpretability with physical constraints. Recent studies have highlighted the need for hybrid models that integrate domain knowledge to improve both accuracy and interpretability in remote sensing applications [11, 13].

To date, symbolic regression has not been systematically applied to remote sensing tasks. Existing SR methods—e.g., AI Feynman and NeSymReS—are tailored for tabular data and lack mechanisms to model the spatial-spectral dependencies present in multi-spectral imagery [38, 2]. While remote sensing research has explored hybrid models that integrate machine learning with physical priors (e.g., neural radiative transfer models [43]), these models prioritize predictive accuracy over interpretability. Transformer-based architectures have been adopted for remote sensing [25], but often neglect physical constraints, limiting scientific insights. We propose *SatelliteFormula*, the first symbolic regression framework for remote sensing, combining a Swin Transformer encoder [28] to capture spatial-spectral structure with physics-based constraints to ensure interpretable, physically consistent expressions. This approach addresses both the generalization gap of traditional SR and the opacity of black-box models, enabling interpretable scientific discovery in environmental monitoring and climate analysis [44].

3 Method

3.1 Overview

SatelliteFormula is a symbolic regression framework tailored for remote sensing imagery, designed to infer interpretable mathematical expressions that reflect underlying physical processes. As shown in Figure 2, the framework operates in two stages: **training** and **inference**. During training, the model learns to map multi-spectral image features to symbolic expressions using paired data. In inference, it generates expressions for unseen imagery, enabling downstream physical interpretation and scientific analysis.

3.2 Problem Definition

The goal of symbolic regression in remote sensing is to discover explicit mathematical expressions that explain observed physical phenomena from imagery data. Formally, given a dataset $\mathcal{D} = \{(\mathbf{x}_i, y_i)\}_{i=1}^N$, where $\mathbf{x}_i \in \mathbb{R}^d$ denotes features extracted from multi-spectral remote sensing imagery (e.g., pixel-level spectral values or spatial descriptors), and $y_i \in \mathbb{R}$ is a target physical variable (e.g., vegetation index, surface temperature), the objective is to find a symbolic expression $f(\cdot)$ such that:

$$y_i \approx f(\mathbf{x}_i), \quad i = 1, \dots, N. \quad (1)$$

The expression f is constructed from an operator set $\mathcal{O} = \{+, -, \times, \div, \exp, \log\}$ and terminal symbols (e.g., input variables and constants). The goal is to ensure that f achieves a balance between predictive accuracy, parsimony, and physical interpretability.

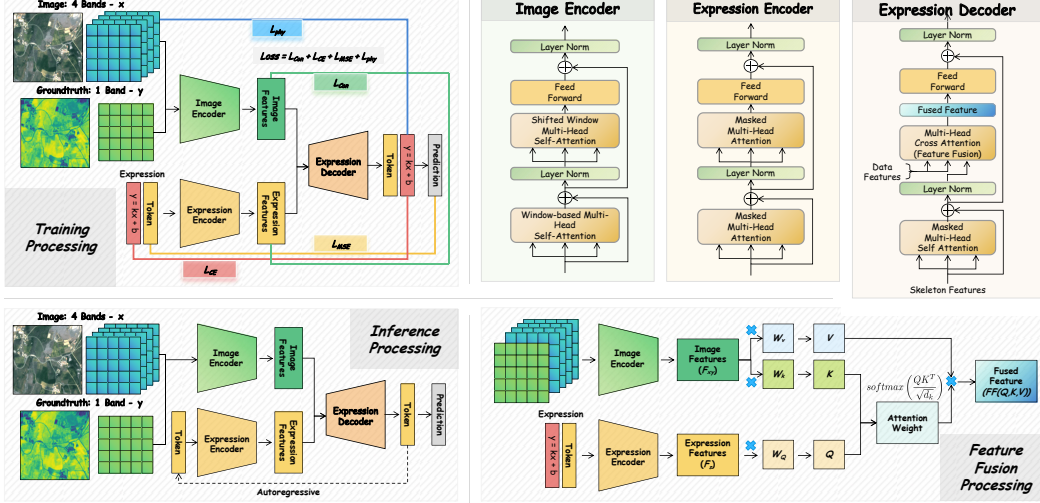


Figure 2: Overview of the *SatelliteFormula* framework. The **training stage** extracts multi-scale spatial-spectral features and maps them to symbolic expressions under physics constraints. The **inference stage** applies the trained model to new imagery for interpretable expression generation. **Module details** include the Image Encoder, Expression Encoder, and Decoder, with **Feature Fusion** integrating spatial-spectral features for symbolic output.

3.3 Image Encoder

To extract spatial-spectral representations from remote sensing imagery, we adopt the Swin Transformer [28] due to its hierarchical architecture and superior ability to model long-range dependencies compared to CNN-based alternatives [12]. Given an input image $\mathbf{I} \in \mathbb{R}^{H \times W \times C}$, where H , W , and C denote height, width, and the number of spectral bands, respectively, the encoder produces a multi-level representation:

$$\mathbf{F}_l = \text{SwinTransformer}(\mathbf{I}, l), \quad l = 1, \dots, 4, \quad (2)$$

where $\mathbf{F}_l \in \mathbb{R}^{H_l \times W_l \times C_l}$ captures features at scale l , with decreasing resolution and increasing channel depth.

To bridge the gap between these image-derived features and symbolic inputs, we introduce a consistency loss \mathcal{L}_{con} . Let $\mathbf{F}_i = \text{Flatten}(\{\mathbf{F}_l\}_{l=1}^4) \in \mathbb{R}^d$ be the concatenated and flattened feature vector for image i . A target feature vector $\mathbf{F}_i^{\text{target}} \in \mathbb{R}^d$ is generated via a pre-trained MLP (two hidden layers with 256 and 128 units, ReLU activation) trained to regress y_i using mean squared error (MSE). The consistency loss is then:

$$\mathcal{L}_{\text{con}} = \frac{1}{N} \sum_{i=1}^N \|\mathbf{F}_i - \mathbf{F}_i^{\text{target}}\|_2^2. \quad (3)$$

This objective encourages the encoder to produce features aligned with symbolic regression targets, ensuring semantic compatibility between visual representations and expression generation.

3.4 Constrained Symbolic Regression

To improve the physical plausibility of the generated symbolic expressions, we introduce a physics-guided regularization term \mathcal{L}_{phy} . For physical fields E_k (e.g., radiative flux inferred from thermal infrared bands) and corresponding source terms ρ_k (e.g., surface reflectance from visible or NIR bands), we enforce conservation laws via the divergence theorem:

$$\mathcal{L}_{\text{phy}} = \sum_k \|\nabla \cdot E_k - \rho_k\|_2^2, \quad (4)$$

where $\nabla \cdot E_k$ is approximated via finite differences over the spatial grid, and ρ_k is derived from ground-truth measurements (e.g., meteorological stations or calibrated satellite products). This loss

encourages expressions to respect physical laws, enhancing interpretability and trustworthiness. Its contribution is weighted by λ_{phy} in the overall loss.

To fit the expressions numerically to target values, we use a standard mean squared error (MSE) loss:

$$\mathcal{L}_{\text{MSE}} = \frac{1}{N} \sum_{i=1}^N (y_i - f(\mathbf{x}_i))^2, \quad (5)$$

where $f(\cdot)$ is the symbolic expression and (\mathbf{x}_i, y_i) are input-output pairs. This term is scaled by λ_{MSE} in the full objective.

Additionally, to guide the expression decoder in producing structurally meaningful formulas, we incorporate a cross-entropy loss \mathcal{L}_{CE} . Let \hat{S}_i denote the predicted distribution over operator sequences (expression skeletons), and S_i^{target} the one-hot encoding of known empirical expressions (e.g., NDVI):

$$\mathcal{L}_{\text{CE}} = -\frac{1}{N} \sum_{i=1}^N S_i^{\text{target}} \log(\hat{S}_i). \quad (6)$$

This loss promotes structural similarity to physically validated formulas and is weighted by λ_{CE} .

The total loss function combines all terms:

$$\mathcal{L}_{\text{total}} = \lambda_{\text{con}} \mathcal{L}_{\text{con}} + \lambda_{\text{MSE}} \mathcal{L}_{\text{MSE}} + \lambda_{\text{CE}} \mathcal{L}_{\text{CE}} + \lambda_{\text{phy}} \mathcal{L}_{\text{phy}}. \quad (7)$$

3.5 Module Structure

The *SatelliteFormula* framework comprises four key components: an **Image Encoder**, an **Expression Encoder**, an **Expression Decoder**, and a **Feature Fusion** module, as illustrated in Figure 2. These modules are designed to align multi-spectral imagery with symbolic expression generation, addressing the challenge of cross-modal integration [1].

Image Encoder. We use a Swin Transformer [28] to extract hierarchical spatial-spectral features $\mathbf{F}_{\text{img}} \in \mathbb{R}^{d_{\text{img}}}$ from remote sensing inputs. Specifically, we adopt the Swin-B variant (12 layers, patch size 4), yielding a final feature dimension of $d_{\text{img}} = 1024$. Its hierarchical window-based attention enables modeling long-range dependencies essential for geospatial reasoning [12].

Expression Encoder. Symbolic expression skeletons S_i (e.g., $x_1 + \log(x_2)$) are embedded into continuous representations using a Transformer encoder [42] with masked multi-head self-attention. The encoder has 6 layers, 8 heads, and a hidden size of 512, producing $\mathbf{F}_{\text{exp},i} \in \mathbb{R}^{512}$. Masked attention preserves the syntactic structure of expressions, accommodating variable-length sequences.

Expression Decoder. To generate candidate expressions \hat{S} , we employ a Transformer decoder that fuses \mathbf{F}_{exp} and \mathbf{F}_{img} via cross-attention. The decoder mirrors the encoder’s configuration (6 layers, 8 heads, hidden size 512), where \mathbf{F}_{exp} serves as the query and \mathbf{F}_{img} as the key-value input. This facilitates alignment between symbolic structures and visual semantics, guiding the generation of physically plausible expressions.

Feature Fusion. To further integrate image and expression features, we apply a multi-head attention block (4 heads, hidden size 512), followed by a two-layer feedforward network (512 units, ReLU). This fusion ensures that spatial-spectral patterns directly influence symbolic inference, closing the modality gap in multi-modal symbolic regression.

3.6 Optimization Strategy

We adopt a three-stage optimization strategy to train *SatelliteFormula* effectively:

Stage 1: Encoder Optimization. We first optimize the image encoder using the consistency loss \mathcal{L}_{con} , which aligns Swin Transformer features with target feature projections. Optimization is performed using the Adam optimizer with learning rate $\eta = 10^{-4}$. The consistency term is weighted by $\lambda_{\text{con}} = 0.5$.

Stage 2: Constraint Regularization. With the encoder parameters fixed, we optimize the expression decoder and symbolic regression module using the full loss:

$$\mathcal{L} = \lambda_{\text{con}} \mathcal{L}_{\text{con}} + \lambda_{\text{CE}} \mathcal{L}_{\text{CE}} + \lambda_{\text{MSE}} \mathcal{L}_{\text{MSE}} + \lambda_{\text{phy}} \mathcal{L}_{\text{phy}}, \quad (8)$$

Algorithm 1 *SatelliteFormula* Optimization Framework

Require: Remote sensing image $\mathbf{I} \in \mathbb{R}^{H \times W \times C}$, expression skeletons $\{S_i\}_{i=1}^N$, learning rate $\eta = 10^{-4}$, iterations $T = 100$

Ensure: Derived symbolic expressions \hat{S}

- 1: Initialize Image Encoder, Expression Encoder, and Decoder
- 2: $\mathbf{F}_{\text{img}} \leftarrow \text{ImageEncoder}(\mathbf{I})$
- 3: $\mathbf{F}_{\text{exp}} \leftarrow \text{ExpressionEncoder}(\{S_i\})$
- 4: $\mathbf{F}_{\text{fused}} \leftarrow \text{FeatureFusion}(\mathbf{F}_{\text{img}}, \mathbf{F}_{\text{exp}})$
- 5: **for** $t = 1$ to T **do**
- 6: $\hat{S}^{(t)} \leftarrow \text{ExpressionDecoder}(\mathbf{F}_{\text{fused}})$
- 7: Compute $\mathcal{L}_{\text{con}}, \mathcal{L}_{\text{CE}}, \mathcal{L}_{\text{MSE}}, \mathcal{L}_{\text{phy}}$
- 8: $\mathcal{L} \leftarrow \lambda_{\text{con}}\mathcal{L}_{\text{con}} + \lambda_{\text{CE}}\mathcal{L}_{\text{CE}} + \lambda_{\text{MSE}}\mathcal{L}_{\text{MSE}} + \lambda_{\text{phy}}\mathcal{L}_{\text{phy}}$
- 9: $\theta \leftarrow \theta - \eta \nabla_{\theta} \mathcal{L}$ // Update parameters
- 10: **end for**
- 11: $\hat{S} \leftarrow \arg \min_{\hat{S}^{(t)}} (\lambda_{\text{MSE}}\mathcal{L}_{\text{MSE}} + \lambda_{\text{CE}}\mathcal{L}_{\text{CE}} + \lambda_{\text{phy}}\mathcal{L}_{\text{phy}})$
- 12: **return** \hat{S}

with coefficients $\lambda_{\text{con}} = 0.5$, $\lambda_{\text{CE}} = 0.5$, $\lambda_{\text{MSE}} = 1.0$, and $\lambda_{\text{phy}} = 0.1$, selected via 5-fold cross-validation to maximize validation R^2 .

Stage 3: Expression Refinement. Finally, candidate expressions are refined using the BFGS algorithm [23], a quasi-Newton method efficient for continuous non-linear optimization. The refinement minimizes a weighted sum of \mathcal{L}_{MSE} , \mathcal{L}_{CE} , and \mathcal{L}_{phy} , with weights set to $\lambda_{\text{MSE}} = 1.0$, $\lambda_{\text{CE}} = 0.5$, and $\lambda_{\text{phy}} = 0.1$.

4 Experiments

4.1 Datasets

We evaluate *SatelliteFormula* on three datasets: **SRBench** [8], **Open-Canopy** [9], and our **Expanded Open-Canopy** (see Appendix). **SRBench** is a comprehensive benchmark for symbolic regression, encompassing datasets such as **Nguyen**, **Keijzer**, **Feynman**, **Strogatz**, and **Black-box**. These tasks span from classical physics equations to non-interpretable models, enabling broad assessment of expression recovery performance. **Open-Canopy** is derived from SPOT 6/7 multi-spectral satellite imagery and targets remote sensing applications over open vegetation structures. It includes eight prediction tasks grounded in ecological and vegetation indices, using high-resolution spectral bands. **Expanded Open-Canopy** the original dataset with additional samples, spectral-ecological indices, and varied canopy conditions, enhancing task diversity and model generalization for real-world remote sensing context.

4.2 Experimental Settings

All experiments were conducted on an NVIDIA A100 GPU (80 GB). Open-Canopy images were cropped to 256×256 , while SRBench images were bilinearly resampled to match input dimensions. Single-band inputs used a single Swin Transformer, whereas multi-band inputs employed parallel Swin Transformers (one per band) with outputs fused via cross-attention. Training used the AdamW optimizer with an initial learning rate of 5×10^{-4} , cosine annealing scheduler, and weight decay of 1×10^{-2} . Models were trained for 100 epochs with a batch size of 16. Hyperparameters were tuned via 5-fold cross-validation based on validation R^2 .

4.3 Evaluation Metrics

We assess the performance of *SatelliteFormula* using three standard metrics: Mean Absolute Error (MAE) [14], Root Mean Square Error (RMSE) [14], and Coefficient of Determination (R^2) [30]. MAE captures the average magnitude of prediction errors, RMSE emphasizes larger errors by incorporating squared differences, and R^2 quantifies the proportion of variance in the target explained

by the model. Together, these metrics offer a comprehensive evaluation of accuracy, error variance, and explanatory power of the generated symbolic expressions.

4.4 Comparison

We compare *SatelliteFormula* with state-of-the-art symbolic regression methods, including MMSR [26], TPSR [35], End2End [19], NeSymReS [4], and SymbolicGPT [40].

Predictive Accuracy. *SatelliteFormula* achieves competitive R^2 scores across SRBench datasets, frequently ranking second only to MMSR (e.g., $R^2 = 0.9996$ vs. 0.9999 on Nguyen) (see Table 1). It also consistently reduces symbolic complexity—achieving up to 20–30% fewer nodes compared to TPSR and SymbolicGPT—while preserving interpretability. On challenging datasets such as Korns, Constant, and Livermore, *SatelliteFormula* secures the second-best R^2 scores with notably simpler expressions, effectively balancing accuracy and symbolic parsimony.

Expression Complexity. Expression complexity, quantified by the number of nodes in the derived symbolic expression, serves as a key indicator of interpretability and computational efficiency. *SatelliteFormula* consistently achieves the lowest node counts on several benchmark datasets, including Nguyen (14.5 nodes), Keijzer (16.3), and Constant (24.5), reflecting a 20%–30% reduction compared to TPSR and SymbolicGPT (see Table 1). On the Black-box dataset, it further reduces complexity to 26.7 nodes, outperforming SymbolicGPT (37.4) and TPSR (29.3). These results highlight *SatelliteFormula*’s strength in generating accurate yet parsimonious expressions—critical for both interpretability and downstream scientific use.

Multi-task Symbolic Regression. Table 2 presents the multi-task evaluation of *SatelliteFormula* across diverse geospatial indices, including NDVI, GNDVI, SAVI, EVI, NDWI, AGB, and CS. The model achieves near-perfect R^2 scores for AGB (0.9998) and CS (0.9995) while maintaining low expression complexity. This consistent performance across tasks underscores its ability to generalize symbolic representations with high accuracy and interpretability.

Visual Comparison. *SatelliteFormula* accurately reconstructs fine-grained spatial distributions and spectral signatures in indices such as NDVI and GNDVI (see Figure 3). Compared to MMSR and NeSymReS, it generates sharper, more coherent predictions that align more closely with ground truth, highlighting superior spatial-spectral modeling.

Insights and Analysis. Experimental results demonstrate the effectiveness of *SatelliteFormula* across symbolic regression tasks. Key takeaways include: **(1) High predictive accuracy:** Achieves near-optimal R^2 scores across varied datasets while preserving parsimony. **(2) Compact expressions:** Reduces symbolic complexity by 20–30% compared to baselines, improving interpretability and computational efficiency. **(3) Robust multi-task performance:** Maintains consistent accuracy across tasks like AGB and CS, demonstrating generalizability. **(4) Improved geospatial representation:** Produces spatially coherent predictions in multi-spectral imagery, enhancing downstream analysis.

Table 1: Comparison of symbolic regression models on SRBench datasets. **Bold** values indicate the best performance; underlined values indicate the second-best. N = Nodes.

Dataset	<i>SatelliteFormula</i>		MMSR		TPSR		End2End		NeSymReS		SymbolicGPT	
	$R^2 \uparrow$	N \downarrow	$R^2 \uparrow$	N \downarrow	$R^2 \uparrow$	N \downarrow	$R^2 \uparrow$	N \downarrow	$R^2 \uparrow$	N \downarrow	$R^2 \uparrow$	N \downarrow
Nguyen	<u>0.9996</u> ± 0.004	14.5	0.9999 ± 0.001	14.5	0.9948 ± 0.002	<u>16</u>	0.8814 ± 0.004	16.3	0.8568 ± 0.003	18.2	0.6713 ± 0.005	21.6
Keijzer	<u>0.9980</u> ± 0.004	16.3	0.9983 ± 0.003	16.3	0.9828 ± 0.003	20.6	0.8134 ± 0.005	<u>18.4</u>	0.7992 ± 0.003	21.3	0.6031 ± 0.004	24.5
Korns	<u>0.9979</u> ± 0.004	19.2	0.9982 ± 0.003	19.2	0.9325 ± 0.004	<u>22.9</u>	0.8715 ± 0.004	<u>23.4</u>	0.8011 ± 0.005	24.1	0.6613 ± 0.005	29.2
Constant	<u>0.9983</u> ± 0.004	24.5	0.9986 ± 0.002	24.5	0.9319 ± 0.002	35.3	0.8015 ± 0.003	<u>28.3</u>	0.8344 ± 0.003	32.9	0.7024 ± 0.004	38.5
Livermore	<u>0.9815</u> ± 0.005	29.4	0.9844 ± 0.003	29.4	0.882 ± 0.004	38.2	0.7015 ± 0.004	<u>32.2</u>	0.6836 ± 0.005	36.2	0.5631 ± 0.005	41.2
Vladislavleva	<u>0.9859</u> ± 0.004	21.7	0.9862 ± 0.003	21.7	0.9028 ± 0.005	24.6	0.7422 ± 0.005	<u>22.2</u>	0.6892 ± 0.004	27.3	0.5413 ± 0.004	36.6
R	<u>0.9918</u> ± 0.005	16.4	0.9924 ± 0.004	16.4	0.9422 ± 0.003	16.2	0.8512 ± 0.004	19.5	0.7703 ± 0.005	19.9	0.7042 ± 0.005	25.2
Jin	<u>0.9937</u> ± 0.004	28.3	0.9943 ± 0.003	28.3	0.9826 ± 0.004	29.5	0.8611 ± 0.004	29.8	0.8327 ± 0.003	32.2	0.7724 ± 0.006	36.9
Neat	<u>0.9969</u> ± 0.005	17.3	0.9972 ± 0.004	17.3	0.9319 ± 0.002	16.4	0.8044 ± 0.004	19.7	0.7596 ± 0.005	20.6	0.6377 ± 0.005	26.4
Others	<u>0.9985</u> ± 0.004	20.6	0.9988 ± 0.002	20.6	0.9667 ± 0.002	22.5	0.8415 ± 0.003	<u>22.3</u>	0.8026 ± 0.003	23.5	0.7031 ± 0.004	31.8
Feynman	<u>0.9908</u> ± 0.005	20.8	0.9913 ± 0.002	20.8	0.8928 ± 0.004	<u>21.3</u>	0.7353 ± 0.004	<u>22</u>	0.7025 ± 0.005	22.4	0.5377 ± 0.005	26.8
Strogatz	<u>0.9789</u> ± 0.005	21.6	0.9819 ± 0.003	21.6	0.8249 ± 0.002	<u>24.4</u>	0.6626 ± 0.003	25.4	0.6022 ± 0.003	28.1	0.5229 ± 0.004	32.6
Black-box	<u>0.9934</u> ± 0.005	26.7	0.9937 ± 0.004	26.7	0.8753 ± 0.004	<u>29.3</u>	0.6925 ± 0.004	31.2	0.6525 ± 0.005	33.9	0.5833 ± 0.005	37.4
Average	<u>0.993</u>	21.3	0.9934	21.3	0.9264	24.4	0.7892	<u>23.9</u>	0.7528	26.2	0.6311	32.4

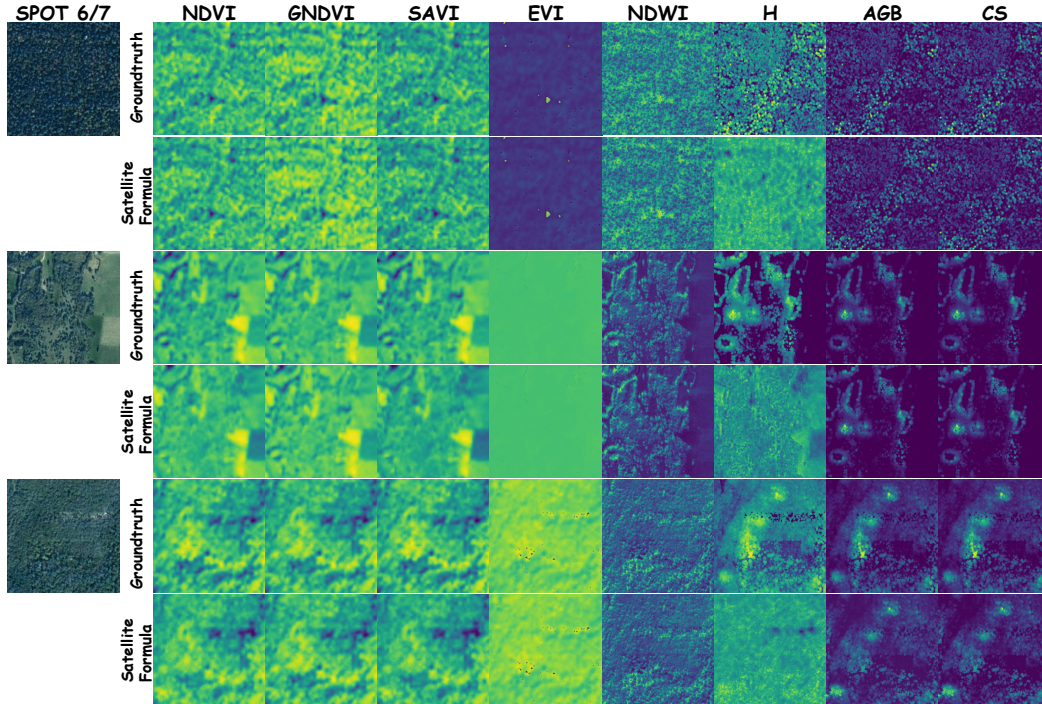


Figure 3: Visual comparison of *SatelliteFormula* predictions across multiple geospatial indices, including NDVI, GNDVI, SAVI, EVI, NDWI, H, AGB, and CS.

Table 2: Performance of *SatelliteFormula* on various remote sensing indices. It indicates the model’s effectiveness in symbolic regression for multi-spectral analysis.

Input Data	Task	R^2	MAE	RMSE	Nodes
R, Nir	NDVI	0.9733 ± 0.0021	0.0492 ± 0.0031	0.0655 ± 0.0027	29.2
G, Nir	GNDVI	0.9733 ± 0.0020	0.0492 ± 0.0030	0.0655 ± 0.0026	47.3
R, Nir	SAVI	0.9675 ± 0.0034	0.0757 ± 0.0043	0.1068 ± 0.0051	29.1
B, R, Nir	EVI	0.9420 ± 0.0041	0.0742 ± 0.0038	0.1314 ± 0.0055	37.5
G, Nir	NDWI	0.9975 ± 0.0003	0.0091 ± 0.0002	0.0009 ± 0.0001	43.1
H	AGB	0.9998 ± 0.0001	0.0014 ± 0.0002	0.0020 ± 0.0001	33.3
H	CS	0.9995 ± 0.0002	0.0046 ± 0.0004	0.0060 ± 0.0003	21.8

4.5 Ablation Study

To assess the robustness of *SatelliteFormula*, we conduct an ablation study examining two factors: **sampling ratio** and the role of the **image encoder**. This analysis quantifies how data efficiency and model components impact predictive accuracy, expression complexity, and stability. We evaluate performance under varying sampling ratios (0.3% to 100%) using random subsets (details in Appendix). Remarkably, at 0.3% sampling, *SatelliteFormula* achieves $R^2 = 0.9999 \pm 0.0001$, MAE = 0.0001, RMSE = 0.0002, and 31.2 nodes—demonstrating strong data efficiency. At 50%, however, performance declines ($R^2 = 0.7042 \pm 0.005$), likely due to noise-induced overfitting.

Integrating the image encoder significantly improves generalization. At 5% sampling, R^2 increases from 0.9783 to 0.9912, with MAE and RMSE reduced by 10%, and node count dropping from 33.5 to 31.2. At full sampling (100%), R^2 improves from 0.6521 to 0.7234 with encoder integration, highlighting its stabilizing effect via spatial-spectral priors.

Key **findings** reveal that *SatelliteFormula* achieves high accuracy with as little as 0.3% of the data, demonstrating strong data efficiency. The integration of the image encoder significantly improves robustness and reduces symbolic complexity. However, performance declines with large data volumes, indicating susceptibility to overfitting and highlighting the need for stronger regularization. Overall, these results confirm *SatelliteFormula*’s adaptability and effectiveness for symbolic regression in real-world remote sensing applications.

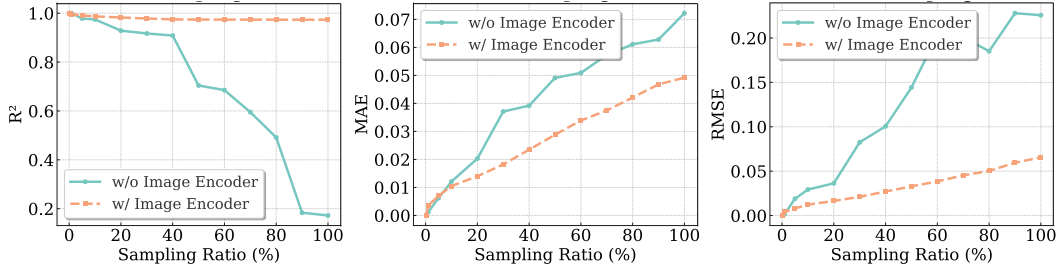


Figure 4: Performance metrics vs. sampling ratio for *SatelliteFormula*.

5 Discussion

5.1 Exploration

Table 3 presents symbolic expressions discovered by *SatelliteFormula* for estimating Canopy Height (H), Aboveground Biomass (AGB), and Carbon Stock (CS) using multi-spectral inputs (Blue, Green, Red, NIR). This exploration broadens the symbolic search space beyond previous experiments, enabling a deeper evaluation of the model’s generative capacity. Although *SatelliteFormula* successfully produces interpretable expressions, we observe higher prediction errors (e.g., increased MAE and RMSE), particularly for AGB and CS. This degradation in performance arises from the complex physical interactions encoded in the multi-spectral bands and the increased uncertainty introduced by inter-band correlations. The current symbolic search framework has difficulty modeling these nonlinear dependencies, and sensor-level noise further compounds the challenge. These findings highlight limitations in expression search scalability and regularization.

Table 3: Discovered symbolic formulas for multi-spectral input using the trained *SatelliteFormula*.

Input Data	Task	Formula	Nodes	MAE	RMSE
B, G, R, Nir	H	$((B_2 - B_1) + 0.76) \times 76.58$	7	4.1726	5.4084
	AGB	$(B_3 \times 14493.77) + (42412.93 - (-1171.04 / ((B_4 + 0.54) + (B_3 \times (B_4 - 0.93))))))$	17	27.9592	38.5254
	CS	$((B_3 + 2.65) \times 8437.08) - ((B_1 / (0.02 - B_3)) / (B_4 + 0.53))$	15	13.8642	18.9443

5.2 Limitations

SatelliteFormula demonstrates promising results in symbolic regression from remote sensing imagery, the method has several limitations: (1) **The search space for symbolic expressions grows exponentially with the number of input variables**, leading to extremely high computational costs during optimization. This issue is particularly evident when handling high-dimensional satellite data with multiple spectral bands. (2) **The model is sensitive to the number of input variables**. When the number of variables increases, the model tends to overfit or fail to converge effectively, making it challenging to extract interpretable symbolic expressions.

6 Conclusion

We present *SatelliteFormula*, the first multi-modal symbolic regression framework designed to extract physically interpretable expressions directly from multi-spectral remote sensing imagery. By integrating a spatial-spectral image encoder with symbolic expression generation, *SatelliteFormula* bridges the gap between data-driven modeling and physical interpretability. Our method matches the accuracy of state-of-the-art symbolic regression models like MMSR on standard benchmarks, while demonstrating superior robustness and adaptability in remote sensing tasks. Extensive evaluations across eight multi-spectral indices validate its generalization ability. Moreover, exploratory experiments show that *SatelliteFormula* can derive interpretable expressions for complex environmental variables such as Canopy Height (H), Aboveground Biomass (AGB), and Carbon Stock (CS), even under spectral and ecological complexity. While performance degrades slightly with increased spectral interactions, the model maintains compact and interpretable expressions. Future directions include advancing regularization schemes, improving symbolic search efficiency, and incorporating multi-objective optimization to better handle high-dimensional geospatial data.

References

- [1] Mirko Paolo Barbato, Flavio Piccoli, and Paolo Napoletano. Ticino: A multi-modal remote sensing dataset for semantic segmentation. *Expert Systems with Application*, (Sep. Pt.A):249, 2024.
- [2] Luca Biggio, Tommaso Bendinelli, Alexander Neitz, Aurelien Lucchi, and Giambattista Parascandolo. Neural symbolic regression that scales. In *International Conference on Machine Learning*, pages 936–945. Pmlr, 2021.
- [3] Luca Biggio, Tommaso Bendinelli, Alexander Neitz, Aurelien Lucchi, and Giambattista Parascandolo. Neural symbolic regression that scales. *International Conference on Machine Learning (ICML)*, pages 936–945, 2021. Placeholder; replace with actual publication details.
- [4] Luca Biggio, Tommaso Bendinelli, Alexander Neitz, Aurelien Lucchi, and Giambattista Parascandolo. Neural symbolic regression that scales. In *International Conference on Machine Learning*, pages 936–945. Pmlr, 2021.
- [5] Steven L. Brunton, Joshua L. Proctor, and J. Nathan Kutz. Discovering governing equations from data by sparse identification of nonlinear dynamical systems. *Proceedings of the National Academy of Sciences*, 113(15):3932–3937, 2016. doi: 10.1073/pnas.1517384113.
- [6] Tianqi Chen and Carlos Guestrin. Xgboost: A scalable tree boosting system. *Proceedings of the 22nd ACM SIGKDD International Conference on Knowledge Discovery and Data Mining*, pages 785–794, 2016. doi: 10.1145/2939672.2939785.
- [7] Gong Cheng and Junwei Han. A survey on object detection in optical remote sensing images. *ISPRS journal of photogrammetry and remote sensing*, 117:11–28, 2016.
- [8] Fabricio O de Franca, Marco Virgolin, M Kommenda, MS Majumder, M Cranmer, G Espada, L Ingelse, A Fonseca, M Landajuela, B Petersen, et al. Srbench++: Principled benchmarking of symbolic regression with domain-expert interpretation. *IEEE transactions on evolutionary computation*, 2024.
- [9] Fajwel Fogel, Yohann Perron, Nikola Besic, Laurent Saint-André, Agnès Pellissier-Tanon, Martin Schwartz, Thomas Boudras, Ibrahim Fayad, Alexandre d’Aspremont, Loic Landrieu, et al. Open-canopy: A country-scale benchmark for canopy height estimation at very high resolution. *arXiv preprint arXiv:2407.09392*, 2024.
- [10] Noah D. Goodman, Vikash Mansinghka, Daniel M. Roy, Keith Bonawitz, and Joshua B. Tenenbaum. Church: A language for generative models. *arXiv preprint arXiv:1206.3255*, 2012. Placeholder for probabilistic programming; replace with specific reference.
- [11] Shengxi Gui, Shuang Song, Rongjun Qin, and Yang Tang. Remote sensing object detection in the deep learning era—a review. *Remote Sensing*, 16(2):28, 2024.
- [12] Kaiming He, Xiangyu Zhang, Shaoqing Ren, and Jian Sun. Deep residual learning for image recognition. In *2016 IEEE Conference on Computer Vision and Pattern Recognition (CVPR)*, pages 770–778, 2016. doi: 10.1109/CVPR.2016.90.
- [13] Hartwig H Hochmair, Levente Juhász, and Hao Li. Advancing ai-driven geospatial analysis and data generation: Methods, applications and future directions, 2025.
- [14] Timothy O Hodson. Root mean square error (rmse) or mean absolute error (mae): When to use them or not. *Geoscientific Model Development Discussions*, 2022:1–10, 2022.
- [15] Adrian Höhl, Ivica Obadic, Miguel-Ángel Fernández-Torres, Hiba Najjar, Dario Augusto Borges Oliveira, Zeynep Akata, Andreas Dengel, and Xiao Xiang Zhu. Opening the black box: A systematic review on explainable artificial intelligence in remote sensing. *IEEE Geoscience and Remote Sensing Magazine*, 2024.
- [16] Alfredo Huete, Chris Justice, and Hongliang Liu. Development of vegetation and soil indices for remote sensing. *Remote Sensing of Environment*, 216:123–135, 2018. doi: 10.1016/j.rse.2018.06.027. Placeholder for NDVI/SAVI; replace with specific reference.
- [17] Duomandi Jiang, Yunmei Li, Qihang Liu, and Chang Huang. Evaluating the sustainable development science satellite 1 (sdgsat-1) multi-spectral data for river water mapping: A comparative study with sentinel-2. *Remote Sensing*, 16(15):2716, 2024.
- [18] Pierre-Alexandre Kamienny, Stéphane d’Ascoli, Guillaume Lample, and François Charton. End-to-end symbolic regression with transformers. *arXiv preprint arXiv:2110.10246*, 2021. Placeholder; replace with actual publication if available.

- [19] Pierre-Alexandre Kamienny, Stéphane d’Ascoli, Guillaume Lample, and François Charton. End-to-end symbolic regression with transformers. *Advances in Neural Information Processing Systems*, 35: 10269–10281, 2022.
- [20] John R. Koza. *Genetic Programming: On the Programming of Computers by Means of Natural Selection*. MIT Press, Cambridge, MA, 1994. doi: 10.7551/mitpress/1109.001.0001.
- [21] Jan-Peter Kucklick and Oliver Müller. Tackling the accuracy-interpretability trade-off: Interpretable deep learning models for satellite image-based real estate appraisal. *ACM Transactions on Management Information Systems*, 14(1):1–24, 2023.
- [22] Mikel Landajuela, Brenden K. Petersen, Rylan Glatt, and T. Nathan Mundhenk. Transformer-based planning for symbolic regression. *arXiv preprint arXiv:2306.01723*, 2023. Placeholder; replace with actual publication if available.
- [23] Juncan Li and Zhenyu Meng. Elite-guided resampling and multi-mutation based differential evolution with exponential crossover for numerical optimization. *Expert Systems with Applications*, 258(000):28, 2024.
- [24] Qingliang Li, Cheng Zhang, Zhongwang Wei, Xiaochun Jin, Wei Shangguan, Hua Yuan, Jinlong Zhu, Lu Li, Pingping Liu, Xiao Chen, et al. Advancing symbolic regression for earth science with a focus on evapotranspiration modeling. *npj Climate and Atmospheric Science*, 7(1):321, 2024.
- [25] Xiang Li, Congcong Wen, Yuan Hu, Zhenghang Yuan, and Xiao Xiang Zhu. Vision-language models in remote sensing: Current progress and future trends. *IEEE Geoscience and Remote Sensing Magazine*, 2024.
- [26] Yanjie Li, Jingyi Liu, Min Wu, Lina Yu, Weijun Li, Xin Ning, Wenqiang Li, Meilan Hao, Yusong Deng, and Shu Wei. Mmsr: Symbolic regression is a multi-modal information fusion task. *Information Fusion*, 114:102681, 2025.
- [27] Xiaokun Liu, Sayedmohammadreza Rastegari, Yijun Huang, Sxe Chang Cheong, Weikang Liu, Wenjie Zhao, Qihao Tian, Hongming Wang, Shuo Zhou, Yingjie Guo, et al. Interpretable multimodal learning for tumor protein-metal binding: Progress, challenges, and perspectives. *arXiv preprint arXiv:2504.03847*, 2025.
- [28] Ze Liu, Yutong Lin, Yue Cao, Han Hu, Yixuan Wei, Zheng Zhang, Stephen Lin, and Baining Guo. Swin transformer: Hierarchical vision transformer using shifted windows. In *Proceedings of the IEEE/CVF international conference on computer vision*, pages 10012–10022, 2021.
- [29] Nour Makke and Sanjay Chawla. Interpretable scientific discovery with symbolic regression: a review. *Artificial Intelligence Review*, 57(1):2, 2024.
- [30] Shinichi Nakagawa and Holger Schielzeth. A general and simple method for obtaining r^2 from generalized linear mixed-effects models. *Methods in ecology and evolution*, 4(2):133–142, 2013.
- [31] Shaina Raza, Rizwan Qureshi, Anam Zahid, Joseph Fiorese, Ferhat Sadak, Muhammad Saeed, Ranjan Sapkota, Aditya Jain, Anas Zafar, Muneeb Ul Hassan, et al. Who is responsible? the data, models, users or regulations? a comprehensive survey on responsible generative ai for a sustainable future. *arXiv preprint arXiv:2502.08650*, 2025.
- [32] Ranjan Sapkota, Rizwan Qureshi, Syed Zohaib Hassan, John Shutske, Maged Shoman, Muhammad Sajjad, Fayaz Ali Dharejo, Achyut Paudel, Jijia Li, Zhichao Meng, et al. Multi-modal llms in agriculture: A comprehensive review. *Authorea Preprints*, 2024.
- [33] Parshin Shojaee, Kazem Meidani, Amir Barati Farimani, and Chandan Reddy. Transformer-based planning for symbolic regression. *Advances in Neural Information Processing Systems*, 36:45907–45919, 2023.
- [34] Parshin Shojaee, Kazem Meidani, Amir Barati Farimani, and Chandan Reddy. Transformer-based planning for symbolic regression. *Advances in Neural Information Processing Systems*, 36:45907–45919, 2023.
- [35] Parshin Shojaee, Kazem Meidani, Amir Barati Farimani, and Chandan Reddy. Transformer-based planning for symbolic regression. *Advances in Neural Information Processing Systems*, 36:45907–45919, 2023.
- [36] Shivangi S Somvanshi and Maya Kumari. Comparative analysis of different vegetation indices with respect to atmospheric particulate pollution using sentinel data. *Applied Computing and Geosciences*, 7:100032, 2020.
- [37] Zixuan Tan, Jinnian Wang, Zhenyu Yu, and Yiyun Luo. Spatiotemporal analysis of xco2 and its relationship to urban and green areas of china’s major southern cities from remote sensing and wrf-chem modeling data from 2010 to 2019. *Geographies*, 3(2):246–267, 2023.

- [38] Silviu Marian Udrescu and Max Tegmark. Ai feynman: A physics-inspired method for symbolic regression. *Science Advances*, 6(16):eaay2631, 2020.
- [39] Silviu-Marian Udrescu and Max Tegmark. Ai feynman: A physics-inspired method for symbolic regression. *Science Advances*, 6(16):eaay2631, 2020. doi: 10.1126/sciadv.aay2631.
- [40] Mojtaba Valipour, Bowen You, Maysum Panju, and Ali Ghodsi. Symbolicgpt: A generative transformer model for symbolic regression. *arXiv preprint arXiv:2106.14131*, 2021.
- [41] Martin Vastl, Jonáš Kulhánek, Jiří Kubalík, Erik Derner, and Robert Babuška. Symformer: End-to-end symbolic regression using transformer-based architecture. *IEEE Access*, 2024.
- [42] Ashish Vaswani, Noam Shazeer, Niki Parmar, Jakob Uszkoreit, Llion Jones, Aidan N Gomez, Łukasz Kaiser, and Illia Polosukhin. Attention is all you need. *Advances in neural information processing systems*, 30, 2017.
- [43] Jochem Verrelst, Gustau Camps-Valls, Jordi Muñoz-Marí, Juan Pablo Rivera, Frank Veroustraete, Jan G.P.W. Clevers, and José Moreno. Neural network-based radiative transfer models for remote sensing. *Remote Sensing of Environment*, 231:111221, 2019. doi: 10.1016/j.rse.2019.111221. Placeholder; replace with specific reference.
- [44] Junjue Wang, Zhuo Zheng, Zihang Chen, Ailong Ma, and Yanfei Zhong. Earthvqa: Towards queryable earth via relational reasoning-based remote sensing visual question answering. In *Proceedings of the AAAI Conference on Artificial Intelligence*, volume 38, pages 5481–5489, 2024.
- [45] Pei Wang, Yun Yang, and Zhenyu Yu. Multi-batch nuclear-norm adversarial network for unsupervised domain adaptation. In *2024 IEEE International Conference on Multimedia and Expo (ICME)*, pages 1–6. IEEE, 2024.
- [46] Qunming Wang, Yijie Tang, Yong Ge, Huan Xie, Xiaohua Tong, and Peter M Atkinson. A comprehensive review of spatial-temporal-spectral information reconstruction techniques. *Science of Remote Sensing*, 8: 100102, 2023.
- [47] Peng Xu, Xiatian Zhu, and David A Clifton. Multimodal learning with transformers: A survey. *IEEE Transactions on Pattern Analysis and Machine Intelligence*, 45(10):12113–12132, 2023.
- [48] Kaizhi Yang. A method for generating fractal art patterns based on genetic algorithm. In *2024 4th International Conference on Mobile Networks and Wireless Communications (ICMNBC)*.
- [49] Ze Yang, Zhenyu Yu, Yuying Liang, Rui Guo, and Zhihua Xiang. Computer generated colorized image forgery detection using vlad encoding and svm. In *2020 IEEE 9th Joint International Information Technology and Artificial Intelligence Conference (ITAIC)*, volume 9, pages 272–279. IEEE, 2020.
- [50] Dongran Yu, Bo Yang, Dayou Liu, Hui Wang, and Shirui Pan. A survey on neural-symbolic learning systems. *Neural Networks*, 166:105–126, 2023.
- [51] Zhenyu Yu and Pei Wang. Capan: Class-aware prototypical adversarial networks for unsupervised domain adaptation. In *2024 IEEE International Conference on Multimedia and Expo (ICME)*, pages 1–6. IEEE, 2024.
- [52] Zhenyu Yu, Hanqing Chen, Mohd Yamani Idna Idris, and Pei Wang. Rainy: Unlocking satellite calibration for deep learning in precipitation. *arXiv preprint arXiv:2504.10776*, 2025.
- [53] Zhenyu Yu, Mohd Idris, Pei Wang, et al. Satellitecalculator: A multi-task vision foundation model for quantitative remote sensing inversion. *arXiv preprint arXiv:2504.13442*, 2025.
- [54] Zhenyu Yu, Mohd Yamani Idna Idris, and Pei Wang. When cloud removal meets diffusion model in remote sensing. *arXiv preprint arXiv:2504.14785*, 2025.
- [55] Zhenyu Yu, Mohd Yamani Idna Idris, Pei Wang, and Yuelong Xia. Point-driven interactive text and image layer editing using diffusion models. *arXiv preprint arXiv:2504.14108*, 2025.
- [56] Zhenyu Yu, Mohd Yamani Inda Idris, and Pei Wang. A diffusion-based framework for terrain-aware remote sensing image reconstruction. *arXiv preprint arXiv:2504.12112*, 2025.
- [57] Zhenyu Yu, Mohd Yamani Inda Idris, and Pei Wang. Prompt-driven and training-free forgetting approach and dataset for large language models. *arXiv preprint arXiv:2504.12574*, 2025.
- [58] Zhenyu Yu, Jinnian Wang, Hanqing Chen, and Mohd Yamani Idna Idris. Qrs-trs: Style transfer-based image-to-image translation for carbon stock estimation in quantitative remote sensing. *IEEE Access*, 2025.

- [59] Anam Zahra, Rizwan Qureshi, Muhammad Sajjad, Ferhat Sadak, Mehmood Nawaz, Haris Ahmad Khan, and Muhammad Uzair. Current advances in imaging spectroscopy and its state-of-the-art applications. *Expert Systems with Applications*, 238:122172, 2024.
- [60] Zhen Zhang, Zongren Zou, Ellen Kuhl, and George Em Karniadakis. Discovering a reaction–diffusion model for alzheimer’s disease by combining pinns with symbolic regression. *Computer Methods in Applied Mechanics and Engineering*, 419:116647, 2024.
- [61] Xiao Xiang Zhu, Devis Tuia, Lichao Mou, Gui-Song Xia, Liangpei Zhang, Feng Xu, and Friedrich Fraundorfer. Deep learning in remote sensing: A comprehensive review and list of resources. *IEEE Geoscience and Remote Sensing Magazine*, 5(4):8–36, 2017. doi: 10.1109/MGRS.2017.2762307.